Some peculiarities of conventional pyrolysis of several agricultural residues in a packed bed reactor

Joan J. Manyà[*]*, Joaquín Ruiz, Jesús Arauzo*

Thermo-chemical Processes Group (GPT), Aragón Institute of Engineering Research (I3A), University of Zaragoza, Maria de Luna 3, E-50018 Zaragoza, Spain.

[*] Corresponding author. Tel: +34-976-762224. Fax: +34-976-761879. E-mail: joanjoma@unizar.es

Abstract

The pyrolytic behavior of four agricultural wastes which are very abundant in Spain (almond shells, wheat straw, grape refuse, and olive stones) has been investigated using a bench scale system. Conventional pyrolysis experiments were performed in a packed bed reactor (58 mm ID) at 5, 10, 15, and 30 K min^{-1} for a final temperature of 923 K. Temperature profiles, conversion times, product yields (gases, liquids, and char), and gas composition have been analyzed to investigate the influence of the biomass composition and the operating conditions on the process. Large differences were noted in the pyrolysis outputs when the heating rate is increased to 30 K min^{-1}. In the case of almond shell samples, higher devolatilization rates accompanied by an increase in secondary charring reactions were observed at 30 K min^{-1}, probably due to the chemical composition of the inorganic fraction present in the almond shells. In addition, when the heating rate is increased to 30 K min^{-1}, the lignin content does not seem substantial effect on the product distribution. This fact suggests that this heating rate value could be a heating requirement in which the majority of pyrolysis does not occur in the low-temperature region.

Keywords

Pyrolysis; Agricultural residues; Principal components analysis; Product distribution.

Introduction

Taking into account the depletion of fossil fuels and the concern of environmental protection, the utilization of biomass resources has attached increasing interest. Pyrolysis is one of the primary thermochemical conversion methods to convert biomass into valuable products (solid charcoal, liquid oil, and gas) in different proportions, depending on the operating conditions (essentially temperature and heating rate) and the biomass composition (hemicellulose, cellulose, lignin, extractives, and mineral matter contents).[1–4] Usually cellulose has the lowest char yield and lignin produces a high char yield.[5] The volatile yield is associated whit that of char, showing the opposite trends.

On the other hand, pyrolysis is also part of the gasification process, which can be separated into two main stages: solid devolatilization (pyrolysis) and char conversion. The char reactivity in the second stage is mainly dependent of the pyrolysis conditions and the amount and composition of the inorganic content. Moreover, the kind of biomass (composition and physical properties) also largely affects both biomass devolatilization and char conversion. In this sense, Di Blasi[6] reported that variations in the physical properties (in particular, the biomass bulk density and the char thermal conductivity) mainly affect the reactivity of secondary reactions of tar vapors and the conversion time.

The knowledge of devolatilization characteristics is needed in order to describe the gasification process. In fact, the temperature dependence of pyrolysis products and the gas composition should be considered when evaluating the potential use of a given biomass feedstock for gasification purposes.

The pyrolysis of some agricultural residues has been studied under different experimental conditions.[1,7–21] There are many factors affecting pyrolysis product yields such as final temperature, particle size, heating rate, reactor type, and initial sample

mass. Miller and Bellan[22] reported that the largest effect of the heating rate was observed in the variation of the conversion times for wood samples. An increase in heating rate decreased both char yield and conversion time. Additionally, the char yields were increasing functions of initial particle size. The char yield increase was related to the activity of the secondary reactions between tar vapors and solid matrix.

Di Blasi et al.[1] compared the product distribution from pyrolysis of wood and several agricultural residues (wheat straw, olive husks, grape refuse, and rice husks). As a result of this study, the authors stated that the product yields and gas composition reproduced trends already observed from wood, but differences were appeared from a quantitative point of view. In this sense, pyrolysis of agricultural residues was always associated with much higher solid yields and lower liquid yields.

Given the critical importance of the devolatilization step in the conversions processes, it is necessary to extend the investigations to other types of residues. On the other hand, further experiments of pyrolysis carried out through packed beds are needed to get a better understanding of the process. In this way, the thermal conditions of the fixed bed reactor should be exactly known.

In this work, the devolatilization behavior of several agricultural wastes typical of Spain (almond shells, wheat straw, grape refuse, and olive stones) has been analyzed. The aim of the study is to investigate the evolution of the mass products yields and gas composition as a function of both biomass composition and operating conditions (mainly temperature, heating rate, and particle size).

Experimental Section

Bench-scale plant. The experimental system used in the conventional pyrolysis experiments is shown in Figure 1. The reactor is inside a 2.5 kW tubular electric furnace

of 32.5 x 10^{-2} m in length, 35.5 x 10^{-2} m in external diameter and 12.0 x 10^{-2} m in internal diameter, connected to a temperature and heating control system. The bed was vertically positioned into the reactor. The sample of biomass was packed in a stainless steel mesh holder (cylindrical-shaped basket) with a diameter of 5.8 x 10^{-2} m and a height of 4.1 x 10^{-2} m. The temperatures at different length and radius inside the sample were measured by means of seven type K thermocouples (OD = 0.5 mm) introduced through the top flange of the reactor. These values are simultaneously monitored by a computerized system. Figure 2 shows the detailed position of the thermocouples in the sample holder. The temperature control is achieved by means of a PID controller which regulates the output power of the furnace. The temperature values provided by the thermocouple T3 (temperature outside the sample) are transmitted as input to the controller.

The pyrolysis of the biomass has been performed applying a nitrogen flow to reduce the bed residence time of volatile pyrolysis products and to ensure an inert reaction environment. The gas leaving the pyrolytic reactor was cooled in two ice condensers, where most of the tar and water are collected. Final cleaning of the gas was performed using a cotton filter. Part of the cleaned gas is diverted to a continuous CO/CO_2 infrared analyzer (ABB A02000, Infrared module Uras 14). Gas production was measured by a volumetric gas meter, taking into account gas temperature and pressure. Finally, the gas composition was determined by means of a micro gas chromatograph (Agilent 3000A, a TCD system equipped with two micro-columns: Porapak N and Molecular Sieve) connected online to the process, giving the volume percentage of N_2, H_2, CO, CO_2, CH_4, C_2H_2, C_2H_4, C_2H_6, and H_2S.

Taking into account the bed depth, the devolatilization process takes place under heat transfer control for all heating rates. For each experiment, a given mass of sample was

uniformly distributed inside the sample basket and positioned in the uniform heated zone of the reactor prior to the experiment and hung at a depth of approximately 20.0 x 10^{-2} m from the top. This vertical position was determined in a previous study[23] to minimize axial temperature profiles. Once the reactor was closed, a nitrogen flow rate of 15 cm^3 NTP s^{-1} (superficial gas velocity referred at 923 K of 0.05 m s^{-1} and gas residence time along the heated zone about 4.5 s) was set by means of a mass flow controller. This value of nitrogen flow rate has been selected according to preliminary tests performed using the same experimental system[23] which indicated that the use of a nitrogen flow rate below 10 cm^3 NTP s^{-1} introduced a significant delay in the gas analysis. The nitrogen flow rate was maintained for 30 min to remove the air from the reaction chamber, and then the experiment started at the selected heating rate (5, 10, 15 or 30 K min^{-1}). When the reactor reached the final required temperature (923 K for all tests), it was kept at this temperature value for a period of time needed to analyze the latest sample gas and to make sure that the pyrolysis process is complete (approximately 20 min). At this point, the reactor was cooled and the char and tar produced were weighted. The mass balance is completed with the integration of the gas species contents over the whole experimental time. More precisely, the mass balance on nitrogen was used to evaluate the gas flow rate.

Materials. Pyrolysis tests, using the experimental system previously described, have been conducted for samples of almond shells, wheat straw, grape refuse, and olive stones. The analyses of the biomass samples are reported in Table 1. The proximate and elemental analyses were performed by the ICB ("Instituto de Carboquímica", CSIC, Zaragoza, Spain). The low heating value (LHV) was also been determined at the ICB using a calorimeter IKA A-2000 (standard procedure: ISO-1928-89).

Extractives (soluble non-structural materials in a biomass sample) percentages were measured following the methodology suggested by the NREL[24] (ASTM E1690-01 and TAPPI T-264 om-88 are similar). This procedure uses a two-step extraction process to remove water soluble and ethanol soluble material. Water soluble materials may include inorganic material, non-structural sugars, and nitrogenous material, among others. On the other hand, ethanol soluble material includes chlorophyll, waxes, or other minor components.

Structural carbohydrates and lignin contents were measured according to procedure proposed by the NREL[25]. This procedure is suitable for free-extractives samples and uses a two-step acid hydrolysis to fractionate the biomass into forms that are more easily quantified. The lignin fractionates into acid insoluble material and acid soluble material. The acid insoluble material may also include ash and protein, which must be accounted for during gravimetric analysis. The acid soluble lignin is measured by UV-Vis spectroscopy. During hydrolysis the polymeric carbohydrates are hydrolyzed into the monomeric forms, which are soluble in the hydrolysis liquid. They are then measured by High Performance Liquid Chromatography.

The main physical properties of the materials used in this study are reported in Table 2. The apparent bulk density of the packed bed becomes an important variable in understanding the heating dynamics of the biomass samples. On the other hand, initial mass values for all biomasses and sizes are also reported.

Results and Discussion

The reproducibility of the measurements was qualitatively checked prior to the execution of the experimental schedule. In this sense, a pyrolysis test was repeated three

times obtaining very similar results (mean relative differences ranged from 1.5% to 5%).

Temperature Profiles. The thermal behavior of the different biomasses while pyrolyzing is analyzed in this section. An example of temporal evolution for the seven temperature measurements described in Figure 2 is shown in Figure 3. For the milled wheat straw samples (0.3–0.5 mm), Figure 4 shows the evolution of the temperature in the center of the sample (T5) as a function of the temperature outside the sample (T3). Significant spatial gradients are observed and, as expected, they become successively higher as more severe heating rates are established. Moisture evaporation could explain the profiles for temperatures below the boiling point of water. For a temperature value ranging between 550 K and 750 K (depending on the heating rate), the temperature inside the sample continuously increased and the profile was maintained parallel to the outside temperature. In addition, temperature values slightly higher than the final steady-state value are observed during the last part of the process. This fact, observed and reported for several researchers in previous works[1,26–28], is probably associated with exothermic lignin degradation.

On the other hand, Figure 5 displays the temperature profiles (for thermocouple placed at the center of the sample, T5) corresponding to two wheat straw samples with different particle size (pellets of 5 mm length and particles sizing in the range 0.3–0.5 mm). From the qualitative point of view, both temperature profiles are similar. Nevertheless, a higher temperature delay was observed for the larger sample size as a result of its higher bulk density (see Table 2). For each material and a given heating rate, no relevant differences in the temperature evolutions were observed when results from two samples with similar bulk densities were compared. This finding confirms the previous results obtained by Di Blasi et al.[1], who observed that the particle size do not

influence the process dynamics and, consequently, the overall process could be controlled by external heat transfer (the interparticle heat transfer resistance dominates over the intraparticle one).

For all experiments performed at heating rates of 5, 10, and 15 K min^{-1} the thermal behavior for the rest of samples (almond shells, olive stones, and grape refuse) was qualitatively similar with quantitative differences in the heating times caused by the different bed properties (in particular, bulk density and char thermal conductivity).

Special attention should be made when analyzing the temperature profiles corresponding to experiments performed at 30 K min^{-1} (see Figure 6). The large temperature gradients observed could be considered as expected due the relatively severe heating rate applied. However, and in contrast to results obtained for the rest of heating rates, clear differences in temperature evolutions have been detected as a function of the solid waste material. Temperature values higher than the temperature outside the sample are observed only for the almond shell and especially for the grape refuse samples. In the case of grape refuse, its lowest bulk density and higher lignin content could explain this behavior. Nevertheless, the largest temperature gradients have been obtained for the olive stone samples in spite of its higher lignin content. This fact suggest that apart from the lignin content and the physical properties of the packed bed, additional factors can play an important role during pyrolysis at moderate heating rates.

In this context, it is well know that the inorganic material strongly influence the biomass pyrolysis process due to its catalytic role.[29–30] In particular, the content and composition (mainly sodium and potassium) of the inorganic material are interpreted as additional catalysts influencing the exothermic secondary reactions, in which additional char is formed by contact between vapor products and solid matrix.[5]

The behavior observed for the almond shell samples could be a consequence of its high potassium and sodium contents (48.7% K_2O and 1.6% Na_2O in total ash) reported by Zevenhoven.[31] The effect related to the composition of the inorganic material could compensate the lower lignin content of this material.

Conversion times. For a given bed depth, heating rate and final temperature; the two main parameters affecting conversion times are the density of the bed and the intrinsic reactivity of the biomass. Additional physical properties such as the char thermal conductivity and the specific heat capacity can weakly affect the conversion time when pyrolysis experiments are performed under external heat transfer control.[6] Conversion time is defined as the operational time elapsed until the 95% of the total gas mass has been released. Table 3 shows the conversion times measured at two heating rates (10 and 30 K min^{-1}) for the milled samples (0.3–0.5 mm). From results reported in Table 3, it is remarkable to observe that variations in the conversion time at 10 K min^{-1} could be partially explained by an increase of the time with apparent bulk density, whereas the unexpected long conversion time for grape residues (with a lower density than both almond shells and olive stones) could be due to a lower intrinsic reactivity. These results are in agreement with those reported in previous studies.[1,6,32]

However, a surprisingly short conversion time has been obtained for almond shell sample at 30 K min^{-1} in spite of its high bulk density. As it was previously mentioned, the nature of the inorganic material present in the almond shell samples may affect the pyrolysis process. In this sense, it is well known that the mineral matter naturally present in the biomass catalyzes the pyrolytic decomposition in an unpredictable variety of ways. [33–34] In the present study, it seems clear that the increase of the devolatilization rate due to catalytic effect of the mineral salts is higher for the highest heating rate tested. Obviously, the decrease of pyrolysis temperature and the subsequent increase of

the devolatilization rate related to the catalytic effect of the mineral matter content are not incompatible with the increasing activity of the charring reactions catalyzed also by inorganic salts.

Product Distribution. Figure 7 shows the product distribution obtained from all experiments performed in a mass basis. From qualitatively analyzing the results displayed in the above-mentioned figure, it is possible to suggest some preliminary considerations regarding the product yields. Regarding the Figure 7a, it seems clear that both heating rate and particle size do not dramatically affect char yields. As expected, taking into account the lignin content, the highest char yields have been obtained from the olive stone samples (see Table 1 to check that the olive stone samples have the highest lignin content). However, almond shells exhibited relatively high char yields in spite of their lower lignin content. In this sense and as previously stated, the inorganic content composition of the almond shells could explain the high char yield as a consequence of the major role played by the secondary char formation.

On the other hand, the Figure 7b clearly reveals an increase of gas yields for experiments heated at 30 K min^{-1}. This increment was especially pronounced in the case of large and medium sized almond shell particles. This fact is in agreement with previous results and considerations regarding the conversion times. The increment of gas yields was associated with a decrease in both liquid and char yields. Nevertheless, in the case of almond shells, the increase of gas yields was at the expense of mainly liquid fraction (see Figure 7c), probably as a consequence of the higher catalytic action of inorganic salts in the secondary charring reactions when the experiments were carried out at 30 K min^{-1}.

In order to reach a more reasoned interpretation of the experimental results concerning to product distribution, Normalized Principal Component Analysis (NPCA)

has been applied to support the interpretation of the data. NPCA is useful for the acquisition of quick information about the similarities in a group of experiments.[35–36] On the other hand, Cluster analysis is another multivariate technique that allows grouping experiments based on similarities using several variables simultaneously.[37] A hierarchical tree in the Cluster analysis calculations can also represent the similarities in a group of results. In this way, a dendrogram connects similar objects by U-shaped lines. The height of each U represents the distance between the two objects being connected. This corresponds to the squared Pearson distances between each pair of observations.[35,38] The Minitab® (v. 14.1) statistical software was used for multivariable analysis calculations.

We selected various data sets with the idea to study the potential influence of the operating variables and sample characteristics. In a first stage, a NPCA calculation was performed individually for each biomass material. The mass product yields (gas, char, and liquid[†]) and the average composition of the main gas species (H_2, CO, CO_2, CH_4, and C_2-hydrocarbons) were included in NPCA calculation. The resulting score plots and dendrograms obtained for the olive stone and almond shell samples are shown in Figures 8–9 (the experiment codes displayed in above-mentioned figures were created by adding the heating rate to the sample code reported in Table 2).

From analyzing the results obtained for the olive stone samples (see Figure 8), it is reasonable to assume that experiments performed at a heating rate in the range from 5 K min^{-1} to 15 K min^{-1} are grouped as a function of the particle size. Nevertheless, different particle sizes seem to have a minor influence for experiments carried out at 30 K min^{-1} whose results obtained using the multivariate methods clearly reveal a high

[†] All of the condensable products collected and weighed (organic compounds and product water formed) are indicated as “liquid”.

degree of differentiation from other experiments performed at 5–15 K min^{-1}. Very similar conclusions about the similarities among pyrolysis experiments have been found for grape refuse and wheat straw samples (for this reason, the score plots and dendrograms for these two samples are not shown). In the case of almond shell samples, the score plot displayed in Figure 9a and corresponding to the principal components' space suggests that the similarities among experiments follow a similar trend as the already observed one for the rest of samples. However, it seems that the effect of particle size could be more pronounced for a given group of experiments. This consideration is illustrated in Figure 9b, where the dendrogram shows a considerable distance of experiments performed using milled almond shells (ASS) with those corresponding to large or medium sample sizes (ASL and ASM). This fact could be related to the potential catalytic role of the inorganic material present in the almond shell samples. In this sense, heat and mass transfer resistance across the particles, when pyrolytic reactions are catalyzed by the inorganic material, might play an important role and could justify the observed differences.

The second stage of the NPCA study is focused on detecting similarities among biomass materials. In this way, a new NPCA calculation was carried out for pyrolysis experiments performed at 5, 10, and 30 K min^{-1} using samples with particle size in the range 0.3–0.5 mm. Figure 10 displays score and dendrogram plots corresponding to this NPC analysis in which three principal components were taken into account since more than 90% of the total variance could not be explained with only two components. In the case of the experiments performed at 5–10 K min^{-1}, the grape refuse and olive stone samples exhibit great similarities, whereas the samples with lower lignin content (almond shells and wheat straw) are grouped at a considerable distance from high lignin content samples. Nevertheless, when the heating rate is increased to 30 K min^{-1}, the

lignin content does not seem substantial effect on the product distribution and gas component yields. This fact suggests that at a heating value of 30 K min^{-1} could be a heating requirement in which the majority of pyrolysis does not occur at low temperatures because the time required to reach the higher temperatures is lower than the case of low heating rates. On the other hand and as was already mentioned in previous section, the catalytic role of the inorganic material present in the biomass seems to be more important when the heating rate increases to 30 K min^{-1}. In fact and in accordance with previous considerations, the almond shell sample clearly reveals a substantial distance from the other samples (at 30 K min^{-1}) probably due to the high catalytic activity of its inorganic salts.

Obviously, NPCA provides qualitative interpretations that should have been confirmed in further studies involving, for example, statistical design of experiments and analysis of variance in order to study the influence (representative under a statistical point of view) of the operating parameters and their possible interaction.

Pyrolysis gas. As it is well known, the producer gas consists basically of CO_2, CO, methane, and lower amounts of hydrogen and C_2-hydrocarbons. Depending on the residence time of the vapors in the heated zone, the activity of the gas phase thermal cracking reactions can alter the gas composition. Despite that the value of gas residence time in the hot zone was low (4.5 s), some differences between the real and the measured gas composition can exist. Table 4 shows the average accumulated yields of CO_2, CO and total gas (in mass percentages) obtained from experiments performed at a heating rate ranged from 5 to 15 K min^{-1} using biomass samples with a particle size distribution in the range 0.3–0.5 mm. In the same table, results corresponding to pyrolysis experiments conducted at 30 K min^{-1} are also displayed for comparison. A considerable decrease of CO_2 contribution (and a subsequent increase of CO more or

less pronounced depending on the biomass feedstock) has been observed when pyrolysis experiments were performed at 30 K min^{-1}. This finding consolidates the hypothesis relative to the major role played by the secondary reactions, which explain the additional release of CO, when the heating rate is fixed at 30 K min^{-1}, probably as a consequence of the higher catalytic activity of the inorganic salts.

The evolution of the gas components as a function of both time and temperature (T5) is shown in Figure 11. The relatively large amount of CO and CO_2 released from all samples is due to the large number of hydroxyl groups and oxygen atoms present in the natural polymers that make up the cell walls (cellulose, hemicellulose, and lignin). The existence of two different regions of significant increase in the CO_2 yields is clearly visible in Figure 11b and is in qualitative agreement with previous studies.[1,3] The high release of carbon dioxide in the low temperature range can be attributed to the specific structural feature of the lignin with high γ–COOH and γ–CO–O-R group content.[39] On the other hand, the successive increase of CO_2 (and CO) yields in the high temperature region could be due to secondary reactions caused by the high reactivity of the vapors and the potential catalytic effect of inorganic species. In the case of almond shell samples, both CO and CO_2 yields increased in the high temperature range as a consequence of the higher activity of the secondary reactions.

Hydrogen is produced by cracking of volatiles and its production is negligible for all biomasses at temperatures below 850 K. On the other hand, the decomposition of methoxyl groups and aliphatic side chains could be the principal formation source of methane and C_2-hydrocarbons. From Figures 11d and 11e, it can be seen that the profiles of CH_4 and C_2-hydrocarbons are very similar. Grape refuse samples exhibit higher methane and C_2-hydrocarbons yields, presumably as a consequence of their high lignin and extractives content. Taking into consideration that olive stone samples (the

material used here with the highest lignin content) evolved much less CH_4 and C_2-hydrocarbons, the amount of extractives can potentially influence the light hydrocarbon yields.

Regarding the yield maxima observed for grape refuse and, in a lower extent, for wheat straw samples (in the operating time ranged from 2200 to 2500 s), two possible reasons can explain this finding: a low intrinsic reactivity in the low temperature region and, in the case of grape refuse samples, the above-mentioned effect related to the high lignin and extractives content.

On the basis of the results reported in this work, it can be suggested that the gas release characteristic is significantly dependent on the type of biomass. In the case of grape refuse, the lower yields of CO and the higher yields of light hydrocarbons and CO_2 are in agreement with those published by Di Blasi et al.[1] for a similar biomass feedstock and could be related to its high lignin content. Nevertheless, results obtained for the olive stone samples are somewhat different than those corresponding to grape refuse in spite of the high amount of lignin present in both original samples. In addition, the gas species yields reported here for the lower-lignin content biomasses (almond shells and wheat straw) do not exhibit similar trends probably due to the high catalytic activity of ions present in the almond shell samples. For all these considerations, it seems difficult to suggest a simplified mathematical correlation (for reactor modeling purposes) between the gas release characteristics and the chemical composition of the biomass (lignin and holocellulose). The extractives content and chemical composition and, especially, the characterization of the inorganic fraction are additional factors to consider.

Conclusions

The devolatilization behavior of four agricultural wastes (almond shells, wheat straw, grape refuse, and olive stones) has been studied using a bench-scale system based on a packed bed reactor (conventional pyrolysis).

As expected, significant spatial gradients are observed when the temperature profiles were analyzed. For heating rates ranged from 5 to 15 K min^{-1}, the thermal behavior was qualitatively similar for all biomasses with quantitative differences in the heating times caused by the different bulk densities. Nevertheless, clear differences in temperature evolutions have been detected as a function of the solid waste material when heating rate was increased to 30 K min^{-1}. At this heating rate value, unexpected temperature profiles were observed. In this sense, additional factors like inorganic fraction characteristics (apart from the lignin content and the physical properties of the bed) can play an important role during pyrolysis process.

Regarding conversion times, the values obtained at a heating rate value of 10 K min^{-1} can be considered as expected and they are basically explained by variations in the bulk density and the intrinsic reactivity. However, a surprisingly short conversion time was measured for almond shells at 30 K min^{-1} in spite of its high bulk density. This result suggests the possibility that the catalytic effect of the mineral salts can be higher when the heating rate is increased and, consequently, the devolatilization rate (and secondary charring reactions) could be increased.

A Normalized Principal Components Analysis combined with Cluster techniques was applied to identify similarities between pyrolysis experiments performed for different biomass feedstocks, particle sizes and heating rates. The results of a first calculation reveal that experiments performed at 5–15 K min^{-1} are grouped as a function of the particle size. Nevertheless, different particle sizes seem to have a minor influence for

experiments carried out at 30 K min^{-1} whose results obtained using the multivariate methods indicate a high degree of differentiation from other experiments performed at 5–15 K min^{-1}. A second stage of the NPCA study provides evidence that for experiments carried out at 5–15 K min^{-1}, the different biomass samples are grouped as a function of their lignin content. Nevertheless, when the heating rate is increased to 30 K min^{-1}, the lignin content does not seem substantial effect on the product distribution. This fact suggests that at a heating rate value of 30 K min^{-1} could be a heating requirement in which the majority of pyrolysis does not occur in the low-temperature region.

Finally, the gas release characteristic is significantly dependent on the type of biomass. Nevertheless and in light of results obtained in the present work, the postulation of a model for the gas release as a function of the biomass chemical composition (lignin and holocellulose) is a very difficult task. In this sense, further studies should be focused on how to quantify the effect of the extractives content and, especially, the inorganic fraction.

Nomenclature

m_0: Initial mass of the sample (kg)

T3: Temperature outside the sample (K)

T5: Temperature in the center of the sample (K)

Acronyms

ASL: Almond Shell sample of large size

ASM: Almond shell sample of medium size

ASS: Almond shell sample of small size (milled)

GRL: Grape refuse sample of large size

GRS: Grape refuse sample of small size (milled)

LHV: Low Heating Value

NPCA: Normalized Principal Components Analysis

NTP: Normal Temperature and Pressure conditions

NREL: National Renewable Energy Laboratory

OSL: Olive stone sample of large size

OSS: Olive stone sample of small size (milled)

TCD: Thermal Conductivity Detector

WSL: Wheat straw sample of large size

WSM: Wheat straw sample of medium size

WSS: Wheat straw sample of small size (milled)

daf: Dry ash free

References

(1) Di Blasi, C.; Signorelli, G.; Di Russo, C.; Rea, G. Product distribution from pyrolysis of wood and agricultural residues. *Ind. Eng. Chem. Res.* **1999**, *38*, 2216–2224.

(2) Várhegyi, G.; Antal, M.J.; Jakab, E; Szabo, P. Kinetic modeling of biomass pyrolysis. *J. Anal. Appl. Pyrolysis* **1997**, *42*, 73–87.

(3) Scott, D.S.; Piskorz, J.; Bergougnou, M.A., Graham, R.; Overend, R.P. The role of temperature in the fast pyrolysis of cellulose and wood. *Ind. Eng. Chem. Res.* **1988**, *27*, 8–18.

(4) Raveendran, K.; Ganesh, A.K., Khilar, C. Influence of mineral matter on biomass pyrolysis characteristics. *Fuel* **1995**, *74*, 1812–1822.

(5) Miller, R.S.; Bellan, J. A generalized biomass pyrolysis model based on superimposed cellulose, hemicellulose and lignin kinetics. *Combust. Sci. Technol*. **1997**, *126*, 97–137.

(6) Di Blasi, C. Influences of physical properties on biomass devolatilization characteristics. *Fuel* **1997**, *76*, 957–964.

(7) Scott, D.S.; Piskorz, J.; Radlein, D. Liquid products from the continuous flash pyrolysis of biomass. *Ind. Eng. Chem. Process Des. Dev.* **1985**, *24*, 581–587.

(8) Wiliams, P.T.; Besler, S. The pyrolysis of rice husks in a thermogravimetric analyzer and static batch reactor. *Fuel* **1993**, *72*, 151–159.

(9) Zanzi, R.; Sjostrom, K.; Bjornbom, E. Rapid high-temperature pyrolysis of biomass in a free-fall reactor. *Fuel* **1996**, *75*, 545–550.

(10) Encinar, J.M.; Beltran, F.J.; Bernalte, A.; Ramiro, A.; Gonzalez, J.F. Pyrolysis of two agricultural residues: olive and grape bagasse. Influence of particle size and temperature. *Biomass Bioenergy* **1996**, *11*, 397–409.

(11) Tsai, W.T.; Lee, M.K.; Chang, Y.M. Fast pyrolysis of rice husks: Products yields and compositions. *Bioresour. Technol.* **2007**, *98*, 22–28.

(12) González, J.F.; Ramiro, A.; González-García, C.M.; Gañán, J.; Encinar, J.M.; Sabio, E.; Rubiales, J. Pyrolysis of almond shells. Energy applications of fractions. *Ind. Eng. Chem. Res.* **2005**, *44*, 3003–3012.

(13) Apaydin-Varol, E.; Pütün, E.; Pütün, A.E. Slow pyrolysis of pistachio shell. *Fuel* **2007**, *86*, 1892–1899.

(14) Zandersons, J.; Gravitis, J.; Kokorevics, A.; Zhurinsh, A.; Bikovens, O.; Tardenaka, A. Studies of the Brazilian sugarcane bagasse carbonization process and products properties. *Biomass Bioenergy* **1999**; *17*, 209–219.

(15) Caballero, J.A.; Conesa, J.A.; Font, R.; Marcilla, A. Pyrolysis kinetics of almond shells and olive stones considering their organic fractions. *J. Anal. Appl. Pyrolysis* **1997**, *42*, 159–175.

(16) Lanzetta, M.; Di Blasi, C. Pyrolysis kinetics of wheat and corn straw. *J. Anal. Appl. Pyrolysis* **1998**, *44*, 181–192.

(17) Demirbas, A. Yields of hydrogen-rich gaseous products via pyrolysis from selected biomass samples. *Fuel* **2001**, *80*, 1885–1891.

(18) Zabaniotou, A.A.; Roussos, A.I.; Koroneos, C.J. A laboratory study of cotton gin waste pyrolysis. *J. Anal. Appl. Pyrolysis* **2000**, *56*, 47–59.

(19) Pütün, A.E.; Ozcan, A.; Gercel, H.F.; Pütün, E. Production of biocrudes from biomass in a fixed-bed tubular reactor: product yields and compositions. *Fuel* **2001**, *80*, 1371–1378.

(20) Islam, M.N.; Zailani, R.; Ani, F.N. Pyrolytic oil from fluidised bed pyrolysis of oil palm shell and its characterisation. *Renew. Energy* **1999**, *17*, 73–84.

(21) Mansaray, K.G.; Ghaly, A.E. Thermal degradation of rice husks in nitrogen atmosphere. *Bioresour. Technol.* **1998**, *65*, 13–20.

(22) Miller, R.S.; Bellan, J. Analysis of reaction products and conversion time in the pyrolysis of cellulose and wood particles. *Comb. Sci. Technol.* **1996**, *119*, 331–373.

(23) Ayllón, M.; Aznar, M.; Sánchez, J.L.; Gea, G.; Arauzo, J. Influence of temperature and heating rate on the fixed bed pyrolysis of meat and bone meal. *Chem. Eng. J.* **2006**, *121*, 85–96.

(24) Ruiz, R.; Scarlata, C.; Sluiter, J.; Templeton, D. *Determination of extractives in biomass*. Document from the National Renewable Energy Laboratory (NREL) of the U.S. Department of Energy; 2005; available online at http://devafdc.nrel.gov/pdfs/9345.pdf.

(25) Sluiter, A.; Hames, B.; Ruiz, R.; Scarlata, C.; Sluiter, J.; Templeton, D.; Crocker, D. *Determination of structural carbohydrates and lignin in biomass*. Document from the National Renewable Energy Laboratory (NREL) of the U.S. Department of Energy; 2006; available online at http://devafdc.nrel.gov/pdfs/9572.pdf.

(26) Shafizadeh, F. Pyrolytic reactions and products of biomass. In *Fundamentals of Thermochemical Biomass Conversion*; Overend, R. P.; Milne, T. A., Mudge, L. K., Eds.; Elsevier: London, 1985; p. 183.

(27) Antal, M. J. Biomass pyrolysis: a review of the literature. Part I. Carbohydrate Pyrolysis. In *Advances in Solar Energy*; Baer, K. W., Duffie, J. A., Eds.; American Solar Energy Society: Boulder, CO, 1982, p. 61.

(28) Antal, M. J. Biomass pyrolysis: a review of the literature. Part II. Lignocellulose Pyrolysis. In *Advances in Solar Energy*; Baer K. W., Duffie, J. A., Eds.; Americam Solar Energy Society: Boulder, CO, 1985; p. 175.

(29) Richards, G. N.; Zheng, G. Influence of Metal Ions and of Salts from Pyrolysis of Wood: Applications to Thermochemical Processing of Newsprint and Biomass. *J. Anal. Appl. Pyrolysis* **1991**, *21*, 133–146.

(30) Antal, M. J.; Várhegyi, G. Cellulose Pyrolysis Kinetics: The Current State of Knowledge. *Ind. Eng. Chem. Res.* **1995**, *34*, 703–717.

(31) Zevenhoven M. *The Prediction of Deposit Formation in Combustion and Gasification of Biomass Fuels, Fractionation and Thermodynamic Multi-Phase Multi-Component Equilibrium (TCPE) Calculations*. Report from the ABO Akademi at Turku (Finland); 2001; available online at http://www.abo.fi/fak/ktf/cmc/publications/reports/01-02.pdf.

(32) Kanury, A. M. Combustion characteristics of biomass fuels. *Combust. Sci. Technol.* **1994**, *97*, 469–491.

(33) Várhegyi, G.; Antal, M. J.; Szekely, T.; Till, F.; Jakab, E. Simultaneous Thermogravimetic-Mass Spectrometric Studies of the Thermal Decomposition of Biopolymers. 2. Sugar Cane Bagasse in the Presence and Absence of Catalysts. *Energy Fuels* **1988**, *2*, 273–277.

(34) Müller-Hagedorn, M.; Bockhorn, H.; Krebs L.; Müller, U. A comparative kinetic study on the pyrolysis of three different wood species. *J. Anal. Appl. Pyrolysis* **2003**, *68–69*, 231–249.

(35) Härdle, W.; Simar, L., *Applied Multivariate Statistical Analysis*, Statistical Series, Springer: New York, 2003.

(36) Mészáros, E.; Jakab, E.; Várhegyi, G.; Szepesváry, P.; Marosvölgyi, B. Comparative study of the thermal behavior of wood and bark of young shoots obtained from an energy plantation. *J. Anal. Appl. Pyrolysis* **2004**, *72*, 317–328.

(37) Ahmedna, M.; Marshall, W.E.; Rao, R.M. Production of granular activated carbons from select agricultural by-products and evaluation of their physical, chemical and adsorption properties. *Bioresour. Technol.* **2000**, *71*, 113–123.

(38) Jackson, J.E. *A User's Guide to Principal Components*, Wiley Series in Probability and Statistics, J. Wiley and Sons: Hoboken, New Jersey, 2003.

(39) Jakab, E.; Faix, O.; Till, F. Thermal decomposition of milled wood lignins studied by Thermogravimetry/Mass spectrometry. *J. Anal. Appl. Pyrolysis* **1997**, *40–41*, 171–186.

Table 1. Ultimate (wt % in a daf basis), proximate (wt %) and chemical analyses (% wt) of agricultural residues.

Biomass	C	H	N	S	O‡	Moisture	Fixed carbon	Volatiles	Ash	Extractives	Structural Carbohydrates	Lignin	LHV (kJ/kg)
Wheat straw	44.3	5.2	0.2	0.1	50.3	8.2	16.8	66.2	8.8	3.8	62.1	17.0	14542
Almond shell	50.2	5.4	0.4	0.0	44.0	8.9	22.2	66.2	2.1	2.1	73.9	21.1	16970
Olive stone	47.1	6.0	2.4	0.2	44.4	8.0	25.1	64.6	2.3	5.0	34.6	31.2	15800
Grape refuse	47.9	6.5	2.9	0.2	42.5	11.5	24.1	56.3	8.1	15.1	34.0	30.4	15257

‡ Obtained by difference

Table 2. Granulometry and bulk density of the packed beds for agricultural residues

	Particle size	Sample code	Apparent bulk density of the bed (kg/m^3)	m_0 (kg)
Wheat straw	Pellets: 5 mm OD, 10 mm Length	WSL	720	0.055–0.060
	Pellets: 5 mm OD, 5 mm Length	WSM	633	0.047–0.055
	0.3–0.5 mm	WSS	372	0.028–0.031
Almond shells	No milled. Particle size in the range 5–30 mm	ASL	558	0.045–0.059
	No milled. Particle size in the range 5–15 mm	ASM	683	0.045–0.055
	0.3–0.5 mm	ASS	770	0.055–0.062
Olive stones	As received. Particle size in the range 0.5–2 mm	OSL	621	0.060–0.064
	0.3–0.5 mm	OSS	749	0.043–0.055
Grape refuse	No milled. Particle size in the range 1–10 mm	GRL	248	0.010–0.020
	0.3–0.5 mm	GRS	547	0.043–0.057

Table 3. Conversion times for the milled samples (0.3–0.5 mm) obtained at two different heating regimes

	Heating rate (K min^{-1})	Conversion time (s)
Wheat straw	10	3176
	30	2300
Almond shells	10	4289
	30	2203
Olive stones	10	4401
	30	2488
Grape refuse	10	5022
	30	2580

Table 4. CO_2, CO and total gas yields for the experiments performed using biomass samples with particle size distribution in the range 0.3–0.5 mm.

	Average accumulated yields (wt % in a daf basis) for experiments conducted at 5–15 K min^{-1}					Accumulated yields (wt % in a daf basis) for experiments conducted at 30 K min^{-1}					Difference (%)			
	CO_2	CO	Total gas	CO_2 contribution to the total gas (%)	CO contribution to the total gas (%)	CO_2	CO	Total gas	CO_2 contribution to the total gas (%)	CO contribution to the total gas (%)	CO_2	CO	CO_2 contribution to the total gas (%)	CO contribution to the total gas (%)
Wheat Straw	15.87 ± 0.90	5.51 ± 0.32	23.76 ± 1.08	66.8	23.2	14.54	6.79	26.54	54.8	25.6	–8.4	23.2	–18.0	10.3
Almond shell	15.71 ± 0.01	5.99 ± 0.45	24.21 ± 0.96	64.9	24.7	13.73	9.18	27.96	49.1	32.8	–12.6	53.3	–24.3	32.8
Olive stone	15.18 ± 0.24	3.37 ± 0.27	21.01 ± 0.18	72.3	16.0	13.88	6.42	25.73	53.9	25.0	–8.6	90.5	–25.4	56.3
Grape refuse	13.92 ± 0.79	3.59 ± 0.04	20.22 ± 0.57	68.8	17.8	15.96	5.28	27.48	58.1	19.2	14.6	47.1	–15.6	7.9

Caption for Figures

Figure 1. Experimental system for conventional pyrolysis experiments. (1), inert gas; (2), mass flow controller; (3), data acquisition; (4), furnace temperature controller; (5), reactor; (6), condensers; (7), cotton filter; (8), thermocouples; (9), CO/CO_2 continuous analyzer; (10), gas chromatograph; (11), gas totalizer meter; (12), exit gas.

Figure 2. Scheme of basket and position of thermocouples inside the sample.

Figure 3. Temperature profiles for milled wheat straw samples (0.3–0.5 mm) at 10 K min^{-1}. The thermocouple numbers correspond to numbers defining the position of each sensor in Figure 2.

Figure 4. Evolution of the temperature in the center of the sample (T5) at different heating rates (solid line, 5 K/min; dashed line, 10 K/min; bold solid line, 15 K/min) for wheat straw samples (0.3–0.5 mm).

Figure 5. Evolution of the temperature in the center of the sample (T5) at different sample sizes (solid line, pellets 5 mm length; dashed line, 0.3–0.5 mm) for wheat straw samples pyrolyzed at 10 K min^{-1}.

Figure 6. Temperature profiles for different biomass samples while degrading at 30 K min^{-1}: (a) wheat straw pellets of 10 mm length; (b) almond shell particles sizing in the range of 5–30 mm; (c) olive stone particles sizing in the range of 0.5–2 mm; (d) grape refuse particles sizing in the range of 1–10 mm.

Figure 7. (a) char, (b) gas, (c) liquid yields (mass % in a daf basis) from pyrolysis of agricultural residues as a function of both heating rate and particle size.

Figure 8. NPC Analysis corresponding to the pyrolysis experiments performed for the olive stone samples: (a) score plot and (b) dendrogram. The first principal component describes 73.2% of the total variance; the second is responsible for 22.2%.

Figure 9. NPC Analysis corresponding to the pyrolysis experiments performed for the almond shell samples: (a) score plot and (b) dendrogram. The first principal component describes 71.5% of the total variance; the second is responsible for 18.6%.

Figure 10. NPC Analysis for the pyrolysis experiments performed using biomass samples with particle size in the range 0.3–0.5 mm : (a) score plot and (b) dendrogram. The first principal component describes 63.9% of the total variance; the second is responsible for 25.2% and the third for 5.4%.

Figure 11. Evolution of (a) CO, (b) CO_2, (c) H_2, (d) C_2 hydrocarbons (C_2H_4 + C_2H_6 + C_2H_2), (e) CH_4 yields (in mass percentages in a daf basis) for experiments performed using biomass samples with particle size in the range 0.3–0.5 mm and heated at 30 K min^{-1} (square, almond shells; circle, grape refuse; cross, wheat straw; up triangle, olive stones).

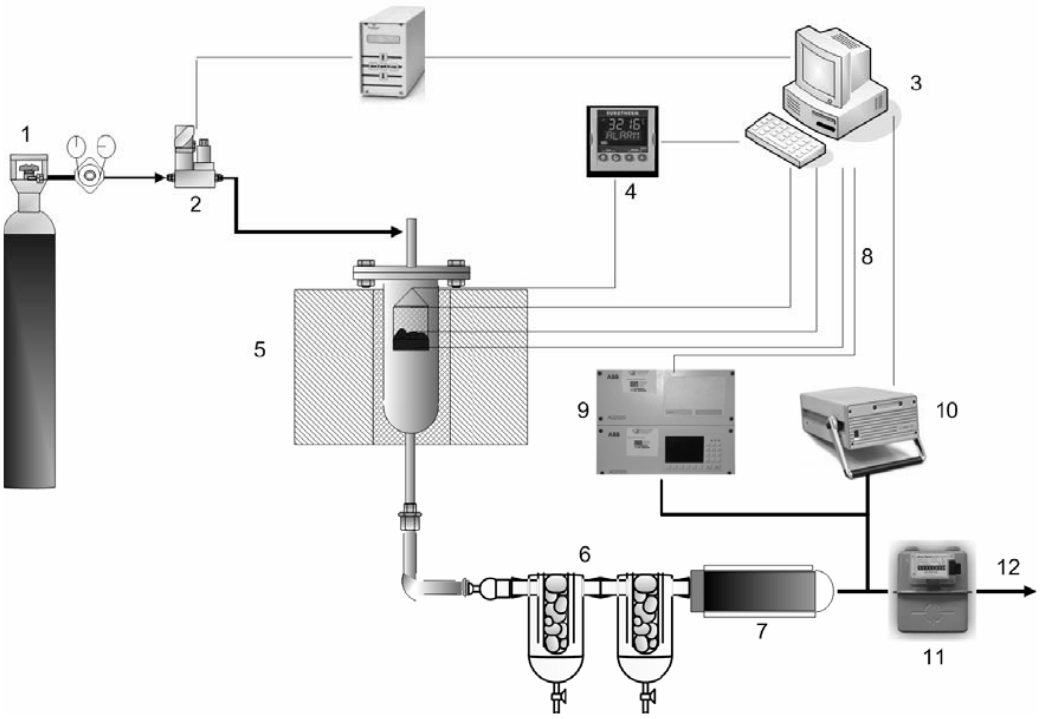

Figure 1

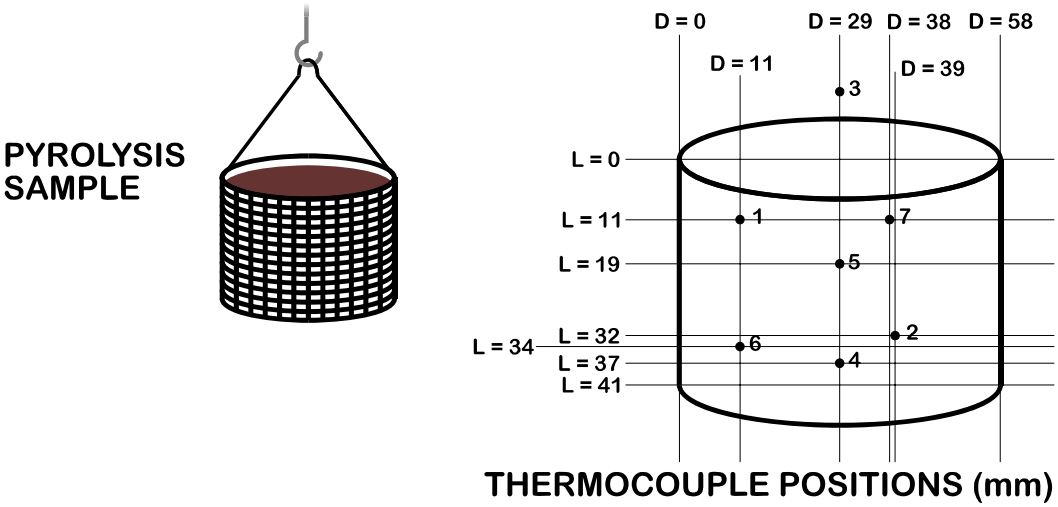
PYROLYSIS
SAMPLE
D = 0
D = 11
D = 29
D = 38
D = 39
D = 58
3
L = 0
L = 11
1
7
L = 19
5
L = 32
2
L = 34
6
L = 37
4
L = 41
THERMOCOUPLE POSITIONS (mm)

Figure 2

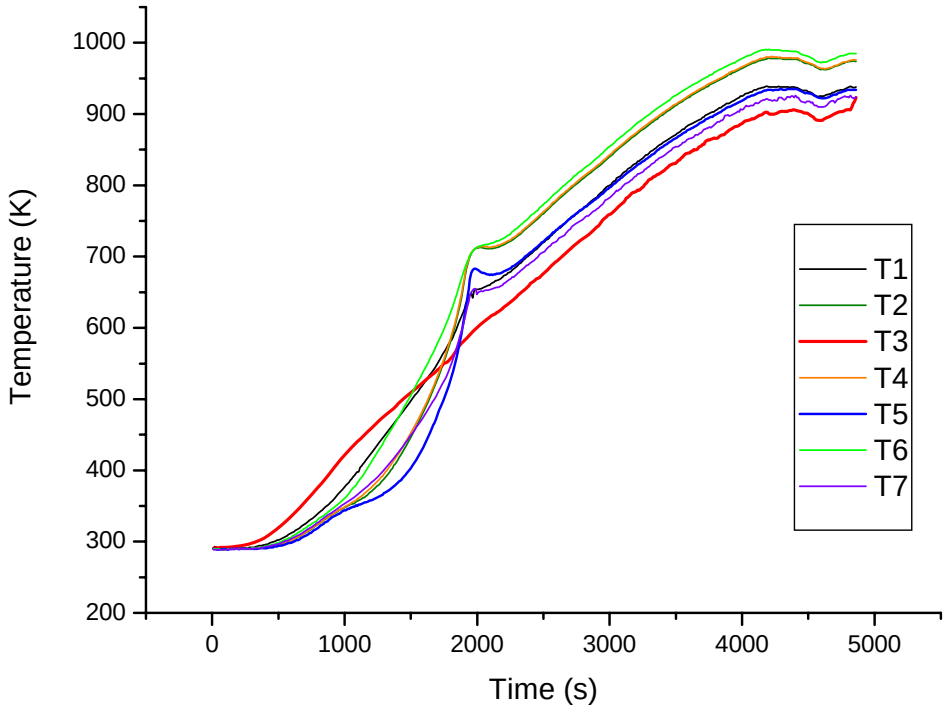
Temperature (K)
1000
900
800
700
600
500
400
300
200
0
1000
2000
3000
4000
5000
Time (s)
T1
T2
T3
T4
T5
T6
T7

Figure 3

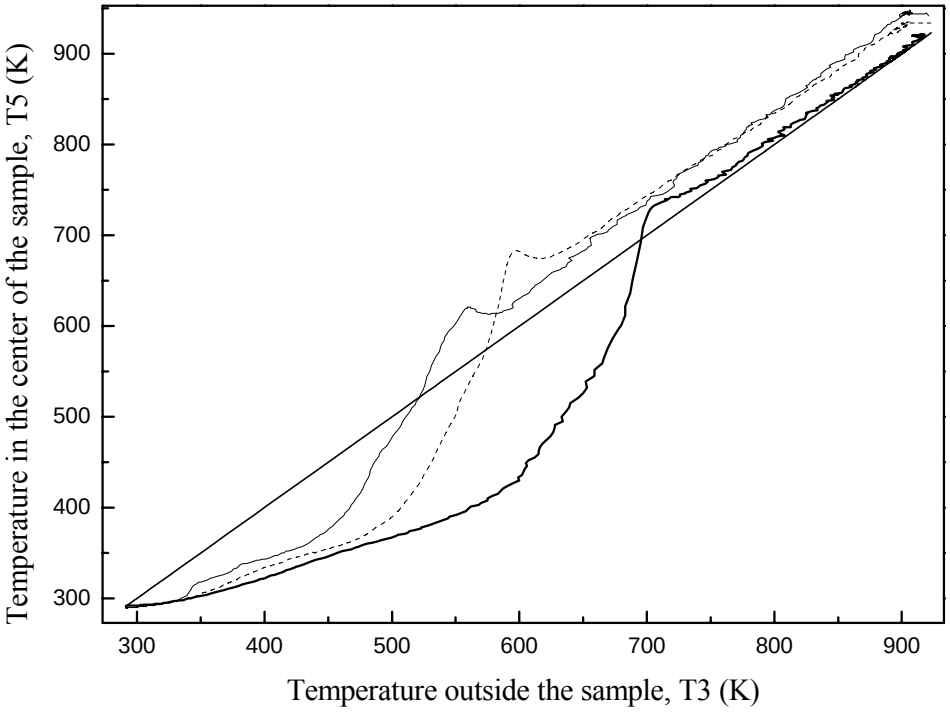
Temperature in the center of the sample, T5 (K)
900
800
700
600
500
400
300
300
400
500
600
700
800
900
Temperature outside the sample, T3 (K)

Figure 4

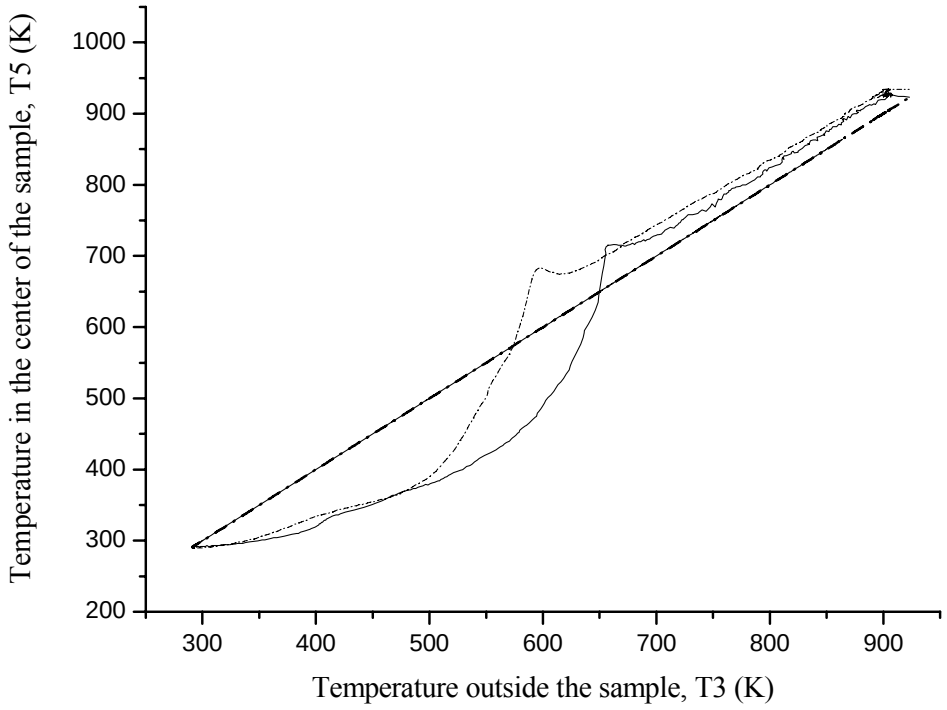
Temperature in the center of the sample, T5 (K)
1000
900
800
700
600
500
400
300
200
300
400
500
600
700
800
900
Temperature outside the sample, T3 (K)

Figure 5

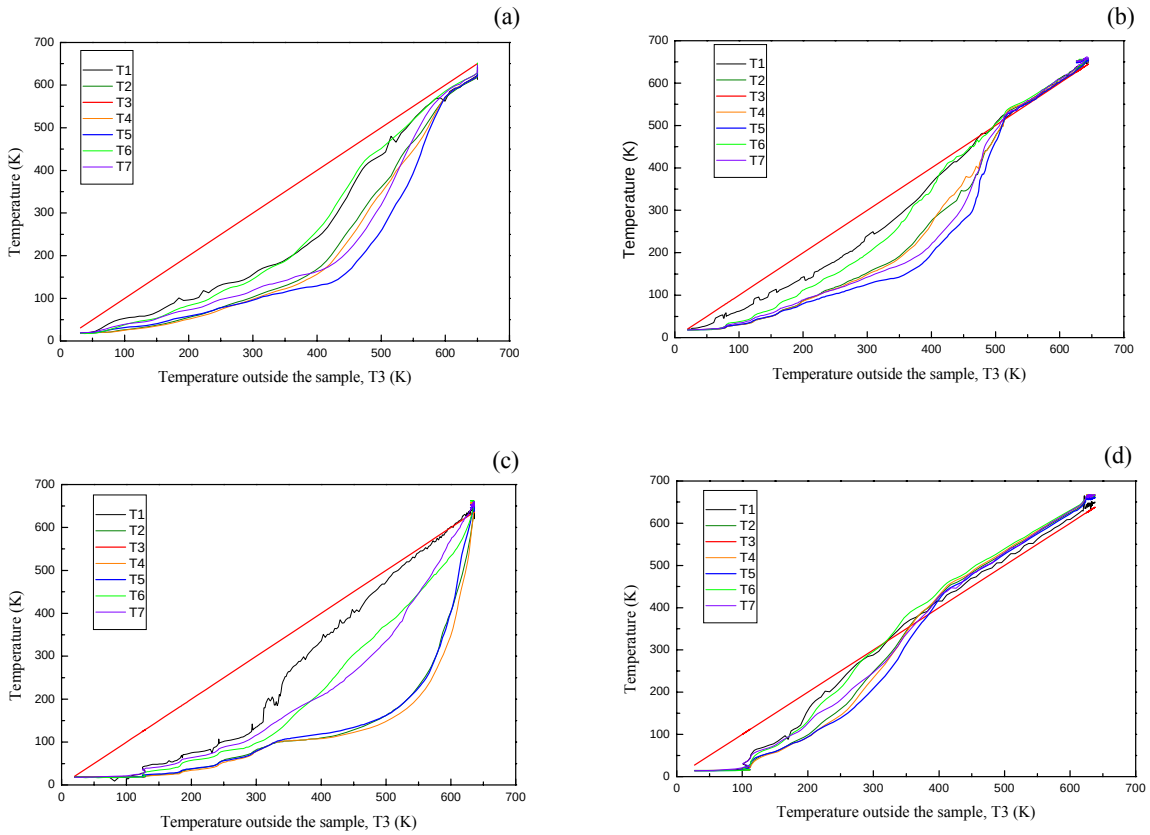
(a)
(b)
(c)
(d)
T1
T2
T3
T4
T5
T6
T7
Temperature (K)
Temperature outside the sample, T3 (K)
0
100
200
300
400
500
600
700

Figure 6

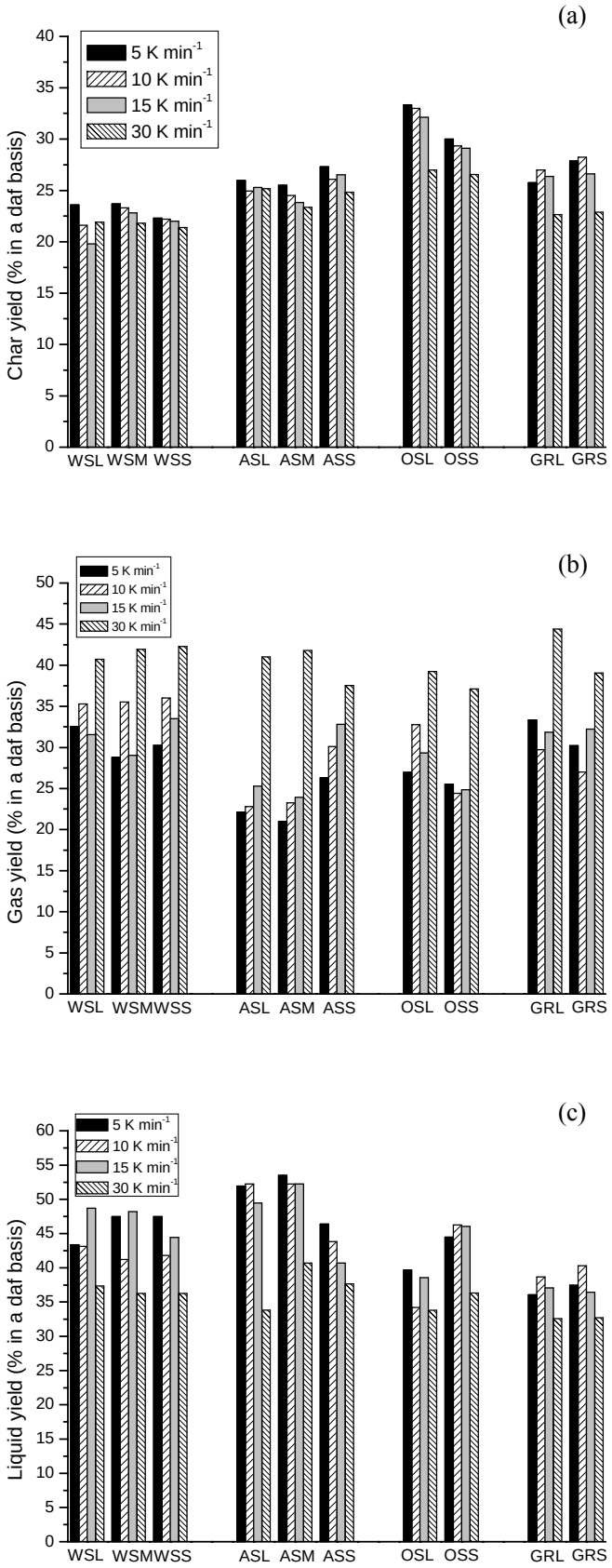
(a)
5 K min-1
10 K min-1
15 K min-1
30 K min-1
Char yield (% in a daf basis)
0
5
10
15
20
25
30
35
40
WSL WSM WSS ASL ASM ASS OSL OSS GRL GRS
(b)
5 K min-1
10 K min-1
15 K min-1
30 K min-1
Gas yield (% in a daf basis)
0
5
10
15
20
25
30
35
40
45
50
WSL WSMWSS ASL ASM ASS OSL OSS GRL GRS
(c)
5 K min-1
10 K min-1
15 K min-1
30 K min-1
Liquid yield (% in a daf basis)
0
5
10
15
20
25
30
35
40
45
50
55
60
WSL WSMWSS ASL ASM ASS OSL OSS GRL GRS

Figure 7

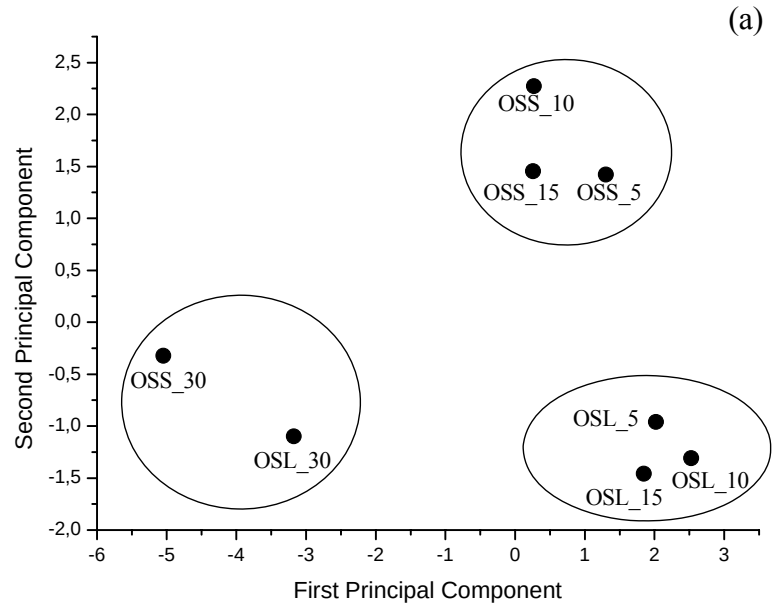
(a)
Second Principal Component
First Principal Component
OSS_10
OSS_15
OSS_5
OSS_30
OSL_30
OSL_5
OSL_10
OSL_15

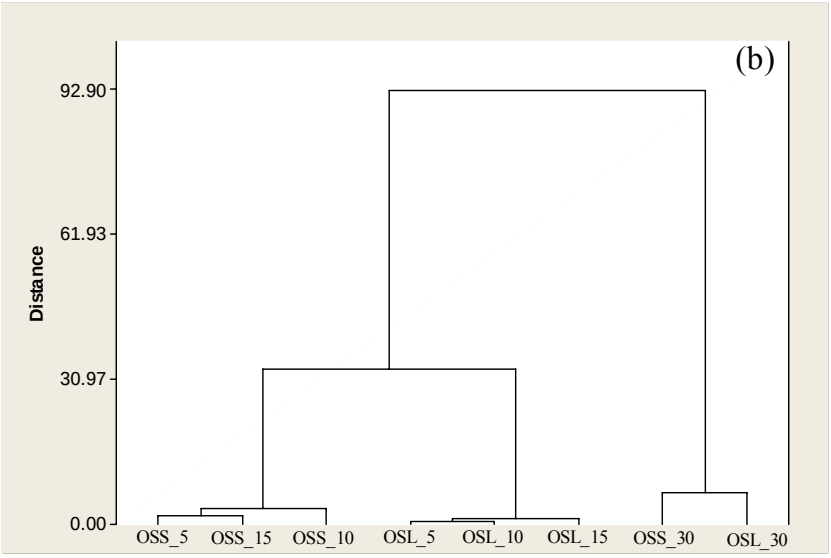
(b)
Distance
92.90
61.93
30.97
0.00
OSS_5
OSS_15
OSS_10
OSL_5
OSL_10
OSL_15
OSS_30
OSL_30

Figure 8

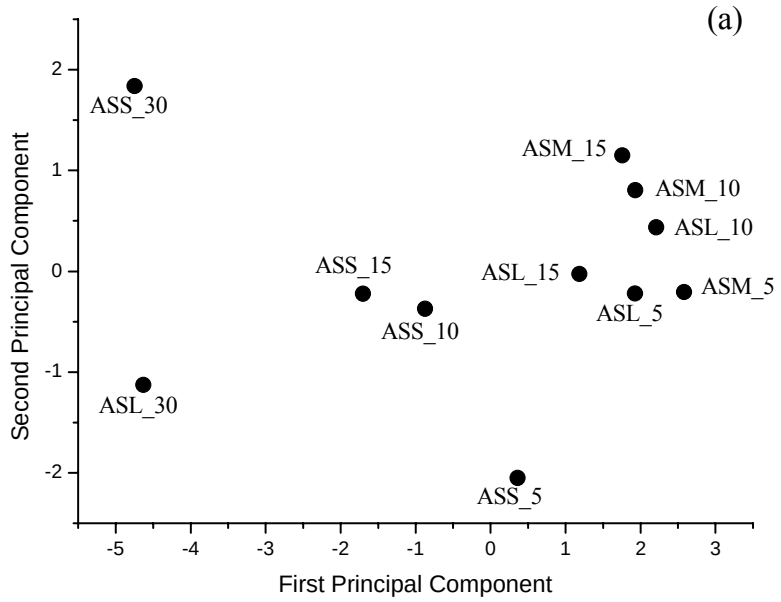
(a)
Second Principal Component
First Principal Component
ASS_30
ASM_15
ASM_10
ASL_10
ASS_15
ASL_15
ASM_5
ASL_5
ASS_10
ASL_30
ASS_5
2
1
0
-1
-2
-5
-4
-3
-2
-1
0
1
2
3

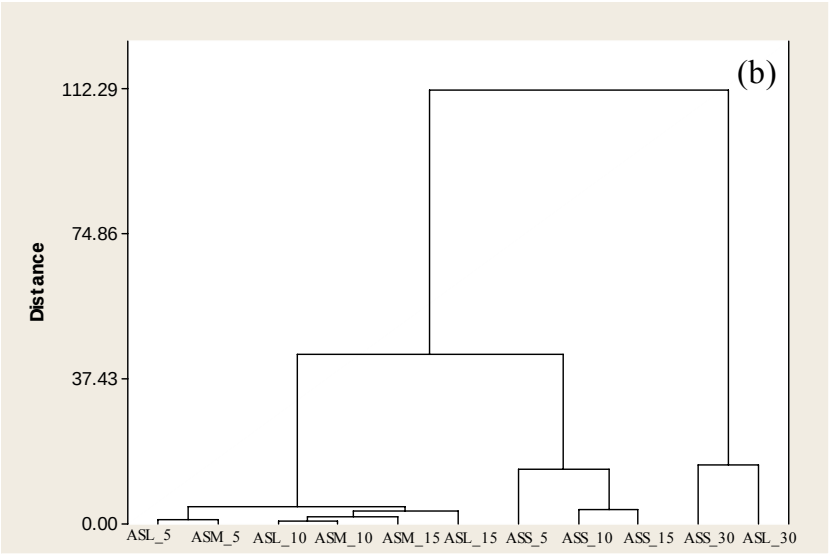
(b)
Distance
112.29
74.86
37.43
0.00
ASL_5
ASM_5
ASL_10
ASM_10
ASM_15
ASL_15
ASS_5
ASS_10
ASS_15
ASS_30
ASL_30

Figure 9

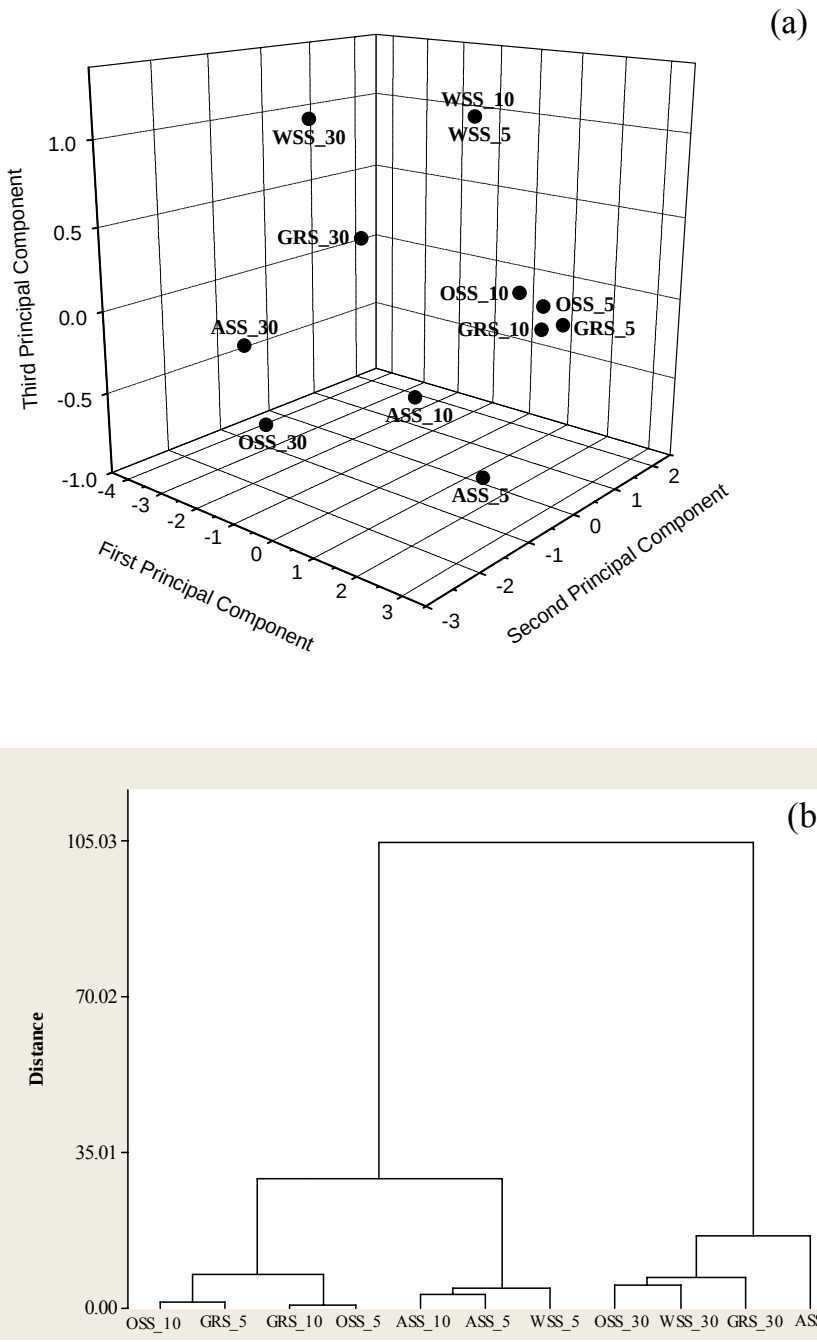
(a)
WSS_10
WSS_5
WSS_30
GRS_30
OSS_10
OSS_5
GRS_10
GRS_5
ASS_30
ASS_10
OSS_30
ASS_5
Third Principal Component
First Principal Component
Second Principal Component
(b)
Distance
105.03
70.02
35.01
0.00
OSS_10 GRS_5 GRS_10 OSS_5 ASS_10 ASS_5 WSS_5 OSS_30 WSS_30 GRS_30 ASS_30

Figure 10

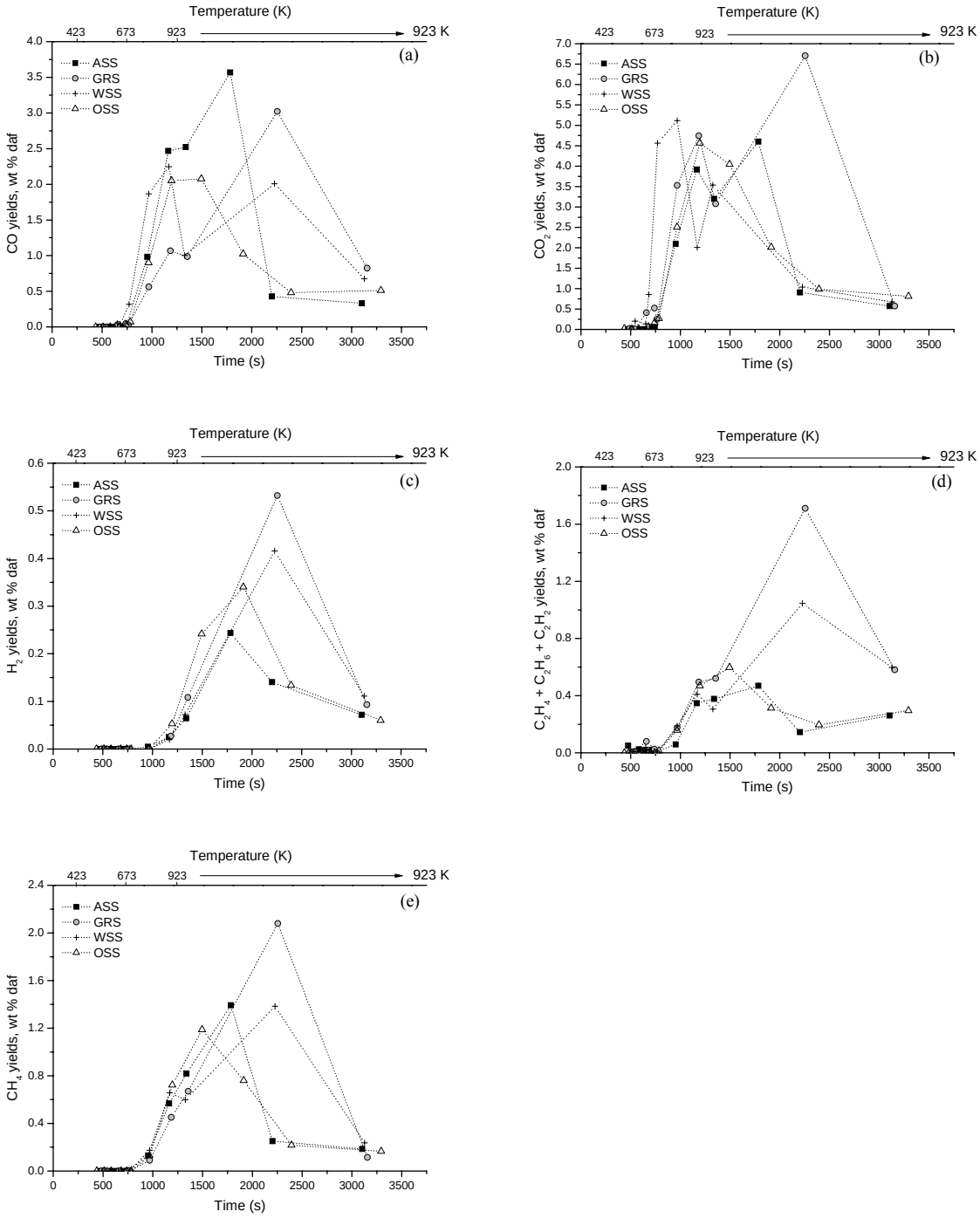
Temperature (K)
423
673
923
923 K
(a)
ASS
GRS
WSS
OSS
CO yields, wt % daf
Time (s)
(b)
CO2 yields, wt % daf
(c)
H2 yields, wt % daf
(d)
C2H4 + C2H6 + C2H2 yields, wt % daf
(e)
CH4 yields, wt % daf

Figure 11